Machine-learning-based classification of shear-band particles in a discrete-element reverse-fault model

Jun KATAGIRI[a,*], Hidetaka SAOMOTO[a], Takayuki SHINOHARA[a]

[a] Integrated Research Center for Resilient Infrastructure, National Institute of Advanced Industrial Science and Technology, 1-1-1 Higashi, Tsukuba, Ibaraki 305-8567, Japan

*Corresponding author (E-mail: j-katagiri@aist.go.jp, ORCID: https://orcid.org/0000-0002-6399-1951)

Authors:

Jun Katagiri: j-katagiri@aist.go.jp
Hidetaka Saomoto: h-saomoto@aist.go.jp
Takayuki Shinohara: shinohara.takayuki@aist.go.jp

Preprint status statement:

This manuscript is a non-peer-reviewed preprint submitted to EarthArXiv. This manuscript is an English preprint version based on a Japanese manuscript prepared for submission to AI and Data Science Proceedings (*AI Data Science Ronbunshu*). It is not the final published version. If the Japanese version is accepted, the final published record will be available via J-STAGE, and the copyright of the published version will belong to the Japan Society of Civil Engineers.

Purpose of posting:

This preprint is shared as an open technical research output to support discussion, verification, and reuse of a simulation-derived machine-learning workflow for interpreting granular fault behavior.

Code and data statement:

The simulation-derived dataset and analysis scripts used for machine-learning classification, permutation-importance analysis, threshold-sensitivity analysis, and figure generation will be made available upon reasonable request.

Machine-learning-based classification of shear-band particles in a discrete-element reverse-fault model

English Translation Draft

Jun KATAGIRI[1], Hidetaka SAOMOTO[1], and Takayuki SHINOHARA[1]

[1]Integrated Research Center for Resilient Infrastructure, National Institute of Advanced Industrial Science and Technology (AIST), Tsukuba, Ibaraki, Japan. Corresponding author E-mail: j-katagiri@aist.go.jp

Preprint status note: *This manuscript is an English preprint version based on a Japanese manuscript prepared for submission to AI and Data Science Proceedings (AI Data Science Ronbunshu). It is not the final published version. If the Japanese version is accepted, the final published record will be available via J-STAGE, and the copyright of the published version will belong to the Japan Society of Civil Engineers.*

Abstract. Discrete element method (DEM) simulations provide time-resolved particle-scale information on particle motion, contact forces, rotation, and local deformation. However, these outputs are high-dimensional, making it difficult to directly interpret which particle-level descriptors characterize localized deformation. This study develops a machine-learning workflow for classifying shear-band particles in a reverse-fault-type DEM model. Shear-band labels are defined using a neighborhood-based local equivalent shear strain, whereas the input features are restricted to low-leakage particle-scale descriptors by excluding the target strain, displacement-derived quantities, and local deformation gradients. A gradient-boosting decision-tree classifier is trained and evaluated using particle-time records as an imbalanced binary classification problem. On the test data, the classifier achieves a PR-AUC of 0.906 and a ROC-AUC of 0.995. Spatial prediction maps show that the classifier captures the localized shear-band structure in the sampled test subset. Permutation importance and ablation analyses indicate that the classification is supported not only by particle position and angular velocity, but also by contact-mechanical, force-related, frictional, and velocity descriptors. These results show that interpretable machine-learning analysis can provide a quantitative summary of particle-scale information associated with shear-band classification in DEM datasets. In an additional threshold-sensitivity analysis, the shear-band labels were redefined using the 90th, 95th, 97.5th, and 99th percentiles while fixing the positive rate at 5% in both the training and test subsets. Angular velocity magnitude, x position, and z position consistently appeared among the top-ranked features, indicating that the main feature-importance trend is not strongly dependent on the specific 97.5th-percentile label threshold.

Keywords: discrete element method; shear band; reverse fault; machine learning; feature importance

1 Introduction

When reverse-fault displacement occurs underground during an earthquake, a localized shear deformation band may form in the subsurface and produce uplift or subsidence at the ground surface. During the 1999 Chi-Chi earthquake in Taiwan, surface fault displacement occurred and caused severe damage to a dam located directly above the fault trace[1]. If such ground deformation occurs beneath important facilities such as transportation infrastructure or nuclear power plants, it can have serious consequences for national economic activity and the lives of nearby residents. Evaluating shear-band formation and ground-surface deformation associated with fault displacement is therefore an important problem.

Localized shear deformation is a common deformation mode in geomaterials, powders, and fault gouges[3, 4, 5, 6, 7]. Previous studies have observed that, within shear bands, particle rearrangement and rotation differ from those of particles outside the shear band. These observations suggest that shear bands should not be understood only as localized zones of large displacement or strain; it is also important to examine how particle-scale state variables, such as particle rotation and velocity, characterize shear-band particles.

The discrete element method (DEM)[8] is a numerical method that can simulate macroscopic deformation behavior of granular materials while simultaneously tracking particle-scale state variables. However, the particle-scale outputs obtained from DEM are high-dimensional, and it has been difficult to efficiently analyze the state variables of all particles over all output times. In previous DEM studies, specific particle-scale state variables were selected and visualized to qualitatively assess their relation to shear-band behavior[3, 4, 5, 6, 7]. In other words, calculating and visualizing shear strain is not equivalent to decomposing the feature groups that contribute to identifying shear-band particles.

In recent years, machine learning has been increasingly applied to microscopic information obtained from DEM simulations and laboratory tests of granular materials and fault gouges, including particle velocity, microslip, and contact states, in order to quantify their relationship with macroscopic frictional states, stress fluctuations, and slip events[9, 10, 11]. For example, Ren et al.[9] showed that machine learning can infer the intermittent frictional state of a sheared granular fault. Ma et al.[10] quantified the relationship between spatial characteristics of microslips and macroscopic stress fluctuations in sheared granular gouges, and Mei et al.[11] showed that spatial clustering of microscopic activity is related to slip avalanches. Reviews and perspectives on machine learning for systems ranging from inter-particle interactions to macroscopic granular flows have also been published, indicating that the integration of granular-material simulations and machine learning is an active research area[12, 13]. In contrast, few studies have classified shear bands caused by reverse-fault displacement at the particle level and analyzed which particle-scale information contributes to distinguishing the inside and outside of the shear band using a feature set that excludes strain- and displacement-derived quantities.

In this study, shear-band labels are defined using the local equivalent shear strain, and therefore the labels themselves can be determined without machine learning. The purpose of introducing a machine-learning model is not to replace this strain-based labeling procedure. Rather, the purpose is to quantify how much information particle-scale state variables such as position, velocity, rotation, contact force, and frictional descriptors contain for distinguishing shear-band particles from non-shear-band particles when the local equivalent shear strain and displacement-derived quantities used to define the labels are excluded from the input. Thus, the classification problem in this study is a data-analysis setting in which known high-strain particle labels are used as the target, and the ability to identify shear-band particles from a set of particle-state variables with relatively high independence from the label definition is evaluated.

Machine-learning methods such as gradient boosting and random forests, which have also been used in the above studies, are widely used for nonlinear classification and feature-importance evaluation[16, 19, 17, 20]. If these methods can be applied to shear-band-particle classification, feature-importance analysis can quantitatively evaluate the contribution of particle-level descriptors to the identification of shear-band particles.

On this basis, the present study examines whether high-strain particles sampled at unseen time steps can be identified from low-leakage particle-scale features within a single reverse-fault DEM condition. Specifically, shear-band-particle labels are defined based on particle-wise local equivalent shear strain, and contemporaneous classification of shear-band and non-shear-band particles is performed using a feature set that excludes quantities directly related to the label, including the local equivalent shear strain, displacement-derived quantities, and local deformation gradients. In addition, permutation importance and ablation analysis are used to evaluate the contribution of each feature group. The objective is not to demonstrate extrapolation to different DEM conditions, forecasting of shear-band initiation, or causal inference. Instead, this study aims to quantitatively summarize interpolation-type classification performance within a single DEM condition and model-dependent feature contributions. The main contribution is not a new machine-learning algorithm but a data-analysis workflow that integrates the design of a low-leakage machine-learning classification problem, performance evaluation, and feature-contribution analysis for high-dimensional DEM particle data in civil and geotechnical engineering.

Table 1: Main conditions of the DEM simulation.

Item	Value
Interparticle contact model	Hertz tangential history
Particle density	2600 kg/m^3
Young's modulus	1.0×10^9 Pa
Poisson's ratio	0.33
Coefficient of restitution	0.5
Particle radius	0.8, 0.9, 1.0, 1.1, 1.2 m
Particle-size weight ratio	0.1, 0.2, 0.4, 0.2, 0.1
Number of particles	250,000
Friction coefficient during packing	0.05
Friction coefficient during reverse-fault simulation	0.5
Time step	1.0×10^{-3} s
Gravitational acceleration	9.81 m/s^2
Velocity of moving wall model	0.05 m/s
Number of shear calculation steps	500,000 steps
Output interval	2,500 steps

2 Methods

2.1 DEM model

The non-commercial general-purpose DEM solver LIGGGHTS-PUBLIC (version 3.8.0) was used. The interparticle contact model was a Hertz-Mindlin tangential-history model[14]. Table 1 summarizes the main simulation conditions and parameter values. The particle density was 2600 kg/m^3, Young's modulus was 1.0×10^9 Pa, Poisson's ratio was 0.33, and the coefficient of restitution was 0.5. Owing to the size of the computational domain, all particles could not be generated at once. Therefore, 62,500 particles were generated in an upper rectangular region of the domain and then allowed to settle under gravity; this process was repeated four times to generate a stable state of 250,000 particles under gravity. During the gravitational deposition process, the friction coefficient was set to 0.05 to produce dense packing. In the subsequent shearing process, the friction coefficient was set to 0.5.

2.2 Local equivalent shear strain

For particle i and its neighboring particles $j \in \mathcal{N}_i$, the relative position vectors at the reference and evaluation times are defined as

$$\boldsymbol{r}_{ij}^0 = \boldsymbol{x}_j^0 - \boldsymbol{x}_i^0, \qquad \boldsymbol{r}_{ij} = \boldsymbol{x}_j - \boldsymbol{x}_i. \tag{1}$$

The local deformation gradient $\boldsymbol{F}_i$ is obtained by least-squares approximation of the relative position change of the neighboring particles as

$$\boldsymbol{F}_i = \left(\sum_{j \in \mathcal{N}_i} \boldsymbol{r}_{ij} (\boldsymbol{r}_{ij}^0)^{\mathrm{T}} \right) \left(\sum_{j \in \mathcal{N}_i} \boldsymbol{r}_{ij}^0 (\boldsymbol{r}_{ij}^0)^{\mathrm{T}} \right)^+ , \tag{2}$$

where $(\cdot)^+$ denotes the Moore-Penrose pseudoinverse. The small-strain tensor is defined as

$$\boldsymbol{\varepsilon}_i = \frac{1}{2}\left[(\boldsymbol{F}_i - \boldsymbol{I}) + (\boldsymbol{F}_i - \boldsymbol{I})^{\mathrm{T}}\right], \tag{3}$$

and the deviatoric strain tensor is defined as

$$\boldsymbol{\varepsilon}_i' = \boldsymbol{\varepsilon}_i - \frac{1}{3}\mathrm{tr}(\boldsymbol{\varepsilon}_i)\boldsymbol{I}. \tag{4}$$

The local equivalent shear strain is then given by

$$e_{\mathrm{eq},i} = \sqrt{\frac{2}{3}\boldsymbol{\varepsilon}_i' : \boldsymbol{\varepsilon}_i'}. \tag{5}$$

In this study, a threshold was assigned to e_{eq}, and particles with e_{eq} greater than or equal to the threshold were identified as shear-band particles.

2.3 Machine-learning dataset and classifier

Each row of the machine-learning dataset corresponds to one particle at one output time, i.e., a particle-time record. The input features include particle position, velocity, applied force, angular velocity, particle radius, number of contacts, local stress-related features, and frictional descriptors derived from contact forces. In contrast, quantities directly related to the shear-band label, including the target local equivalent shear strain, displacement, and local deformation gradient, were excluded from the input.

A gradient-boosting decision-tree classifier was used. The model output is the probability that a particle belongs to the shear band. The data were split into training and test sets based on output time. From the training-time group, 150,000 rows were sampled, and from the test-time group, 50,000 rows were sampled. The positive rate was adjusted to 5% in both sets. This adjustment is a sampling procedure for performance evaluation; therefore, the predicted probabilities shown in this paper should be interpreted as classification scores under the sampling condition rather than as the prior probability of shear-band particles in the full particle set. In addition, the test in this study evaluates classification performance at unseen time steps within the same DEM condition, and it does not evaluate extrapolation to different fault angles, boundary conditions, or particle-size distributions. Classification performance was evaluated using precision, recall, F1 score, ROC-AUC, and PR-AUC. Because the data are imbalanced with few positive samples, PR-AUC was calculated in addition to ROC-AUC[18].

To examine the robustness of feature importance to the shear-band-label threshold, labels were redefined using four thresholds: the 90th, 95th, 97.5th, and 99th percentiles. A classifier was retrained for each label definition. In this supplementary analysis, all conditions other than the threshold were aligned with the main classification model: the same time-based split, feature set, and learning settings were used, and the positive rate was fixed at 5% in both the training set of 150,000 rows and the test set of 50,000 rows. This setting was intended to make differences in classification performance and feature importance arise primarily from the label-threshold definition.

Table 2: Main feature sets used in the ablation analysis.

ID	Feature set
A0	All low-leakage features
A1	Angular velocity removed
A2	Position removed
A3	Motion, force, angular velocity, and position removed
A4	Position and angular velocity removed
A5	Contact, stress, friction, and force features only
A6	Contact and friction features only

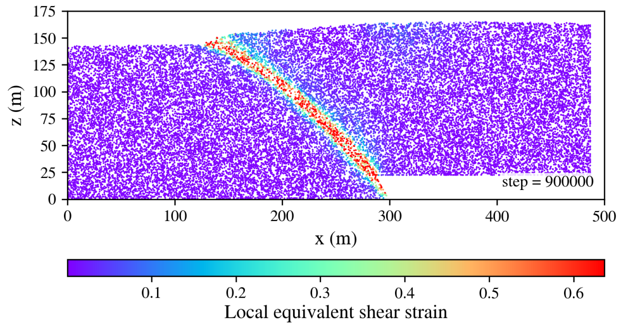

Figure 1: Spatial distribution of local equivalent shear strain in the final state of the reverse-fault simulation.

2.4 Feature importance and ablation analysis

Feature importance was evaluated by permutation importance[20]. This method evaluates the predictive contribution of a feature by measuring the decrease in classification performance when the values of that feature are randomly permuted. To examine the contribution of feature groups, ablation analysis was conducted using the feature sets shown in Table 2. In this paper, ablation analysis means comparing the decrease in predictive performance when specific features are removed. By removing position information and angular-velocity information, we examined whether the classification performance could be explained only by the spatial localization of the shear band or by strong particle rotation.

3 Results and discussion

3.1 Spatial distribution and frequency distribution of shear strain

Figure 1 shows the spatial distribution of e_{eq} in the final state of the reverse-fault-displacement simulation. The particles shown in red correspond to the vicinity of the localized shear deformation band expected to form owing to reverse-fault displacement. In other words, the red region occupies only a small area relative to the whole domain, while most of the domain does not experience large shear strain.

In the upper tail of the frequency distribution, rather than around its high-frequency peak, the high-value range on the right-hand side of the distribution can be regarded as representing the shear band.

Figure 2 shows the frequency distribution of e_{eq} in the fi-

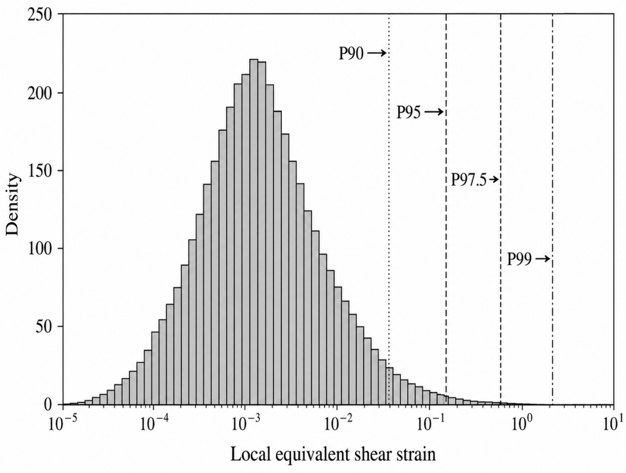

Figure 2: Frequency distribution of local equivalent shear strain in the final state of the reverse-fault simulation.

nal state of the reverse-fault-displacement simulation. Although the figure shows only the final-state distribution, similar frequency distributions were confirmed at multiple time stages. As shown in the spatial distribution in Fig. 1, the area of high local equivalent shear strain is concentrated in a very narrow region compared with the whole domain. Thus, in Fig. 2, the high-value tail on the right-hand side of the distribution, rather than the high-frequency region around the peak, can be interpreted as representing the shear band.

3.2 Threshold sensitivity

Based on the frequency distribution shown in Fig. 2, particles with strain values greater than a certain threshold were identified as particles located inside the shear band. Four candidate thresholds were examined for identifying shear-band particles: the 90th, 95th, 97.5th, and 99th percentiles. These four thresholds are not physically derived; instead, they were used as trial candidates for the high-value tail of the distribution. Figure 2 also shows vertical lines corresponding to the 90th, 95th, 97.5th, and 99th percentiles. The positions of these lines indicate that even the lowest candidate threshold, the 90th percentile, selects only a small fraction of all particles as shear-band particles.

Figure 3 shows the spatial distribution of shear-band particles when the threshold is changed to the 90th, 95th, 97.5th, and 99th percentiles. In the figure, shear-band particles are shown in black, and non-shear-band particles are shown in gray. As expected, a lower threshold results in more particles being classified as shear-band particles. The region shown in red in Fig. 1 corresponds to the main fault. For the 90th and 95th percentile thresholds, a localized region of shear deformation that can be interpreted as a secondary fault also appears near the ground surface to the upper right of the main fault in the figure. The occurrence of main and secondary faults in this positional relationship has also been confirmed in previous model experiments and simulations[2].

Figure 3 shows that, for all four threshold candidates, the shear band corresponding to the main fault can be extracted.

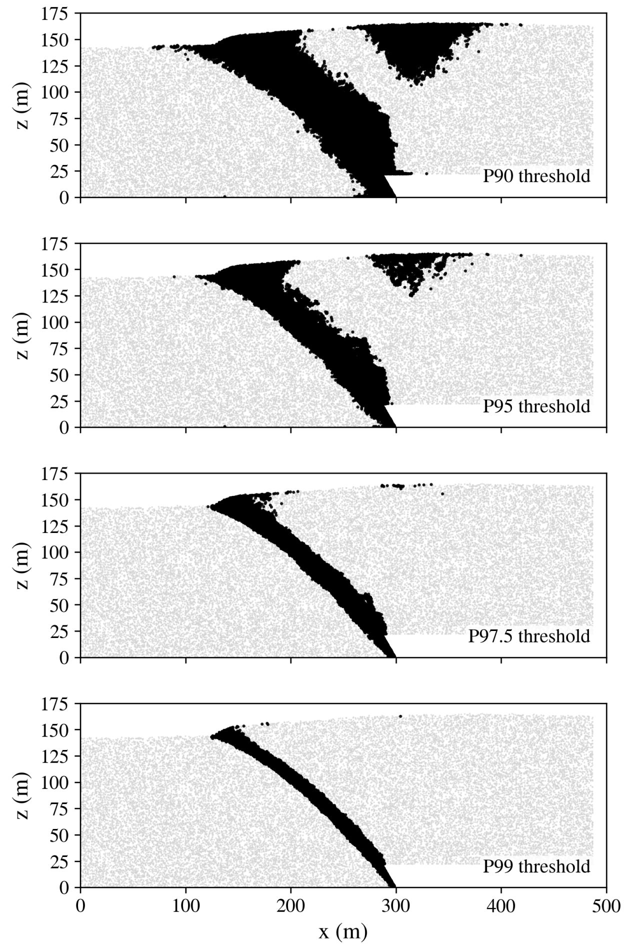

Figure 3: Threshold sensitivity based on the local equivalent shear strain.

However, the apparent width of the main shear band differs with the threshold. In addition, in the 90th and 95th percentile cases, the region interpreted as a secondary fault is also extracted, whereas in the 97.5th and 99th percentile cases, this secondary-fault region is hardly extracted.

The focus of this paper is to construct a workflow for extracting a shear band from DEM results and evaluating the phenomenon using machine learning. Therefore, the 97.5th percentile was used on a trial basis for the subsequent machine-learning analysis. An important future task is to evaluate, through experimental validation, which threshold most appropriately represents the shear band.

Representative particle-scale features such as angular velocity, interparticle force, number of contacts, frictional descriptors, and velocity were confirmed to show characteristic spatial distributions around the shear-band region shown in black in Fig. 3. In this paper, rather than presenting these feature distributions visually, quantitative evaluations based on classification performance, spatial prediction probability, permutation importance, and ablation analysis are presented.

Table 3: Performance of the main classification model.

Metric	Value
PR-AUC	0.906
ROC-AUC	0.995
Precision at threshold 0.9	0.816
Recall at threshold 0.9	0.838
F1 at threshold 0.9	0.827

3.3 Prediction results of the main classification model

The main classification model achieved a PR-AUC of 0.906 and a ROC-AUC of 0.995 on the test data. When the predicted probability threshold was set to 0.9, precision, recall, and F1 score were 0.816, 0.838, and 0.827, respectively. These results show that shear-band particles can be identified with high classification performance within this DEM condition using particle-scale features other than the local equivalent shear strain.

Figure 4 shows the true shear-band labels, binary classification results obtained using the machine-learning model, and the spatial distribution of the predicted probability of being a shear-band particle for the sampled test data. The true labels in the upper panel correspond to the particle group in the high-value range above the 97.5th percentile of the local equivalent shear strain distribution described above.

The binary classification result in the middle panel was obtained using a predicted-probability threshold of 0.9. The predicted shear-band particles approximately coincide with the shear band indicated by the true labels in the upper panel. This indicates that the model did not sporadically detect isolated particle groups but instead extracted a spatially continuous localized shear-deformation region. However, differences from the true labels are observed in parts of the shear-band boundary. These differences are inferred to arise from the setting of the probability threshold; the classification near the shear-band boundary is uncertain and threshold-dependent.

In the lower panel showing the predicted probability distribution, high predicted probabilities are concentrated along the shear band indicated by the true labels, while low-probability particles are widely distributed in the surrounding non-shear-band region. Particles with intermediate predicted probabilities are also present near the shear-band margin, especially from the upper to central parts of the band. This indicates that uncertainty near the shear-band boundary, which is difficult to represent using binary labels alone, can be expressed continuously as predicted probability. These results confirm that the classification model can extract the spatially localized shear-band structure from particle-scale features.

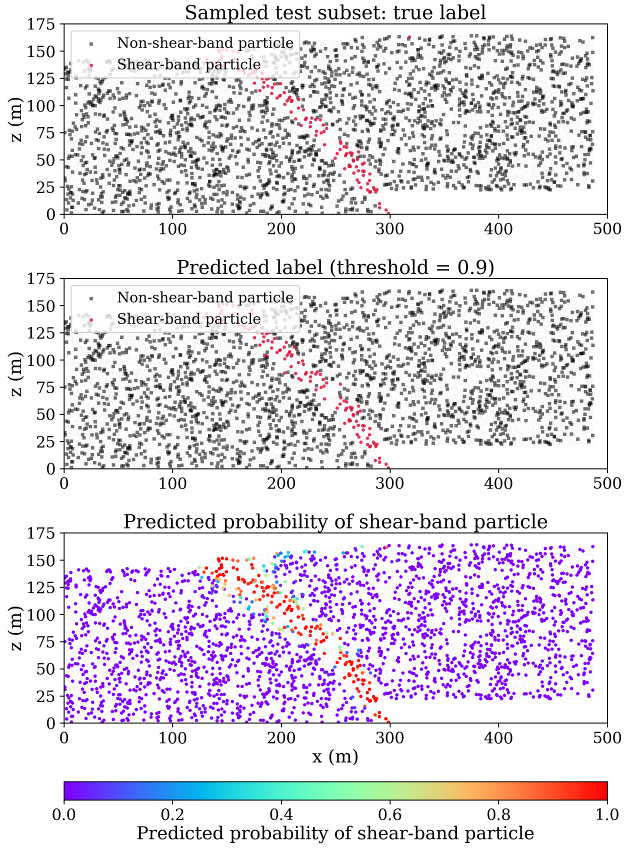

Figure 4: True labels of shear-band particles in the sampled test data at the final step (top), binary classification result obtained by the machine-learning model (middle), and spatial distribution of the predicted probability of being a shear-band particle (bottom).

3.4 Feature importance and ablation

Figure 5 shows the major feature importances based on permutation importance. Only features with relatively large permutation importance are shown. Features not shown had importance values of 0.001 or less and were judged to have relatively small contributions.

Figure 5 shows that angular velocity magnitude has the highest importance, followed by position, applied force, number of contacts, and velocity. This result indicates that the classification of shear-band particles is supported by a combination of kinematic, contact-mechanical, and frictional information rather than by a single feature group alone. The high importance of angular velocity is consistent with previous studies that emphasized the role of particle rotation in shear-band formation[4, 5].

To examine the influence of the shear-band-label threshold on feature importance, labels were redefined using the 90th, 95th, 97.5th, and 99th percentile thresholds, and a classifier was retrained for each threshold after fixing the positive rate to 5% in both the training and test subsets. The results are shown in Table 4. The PR-AUC values ranged from 0.825 to 0.906, and the best F1 scores ranged from 0.740 to 0.835. Thus, high-strain particles and other particles could be distinguished with at least moderate to high performance for all thresholds. In particular, for the 97.5th percentile, the PR-AUC was 0.906, reproducing the result of the main classification model shown in Table 3. Regarding the top-ranked features, the P90 case ranked x position, angular velocity magnitude, and z position in that order. For P95, P97.5, and P99, angular velocity magnitude, x position, and z position consistently appeared as the top three

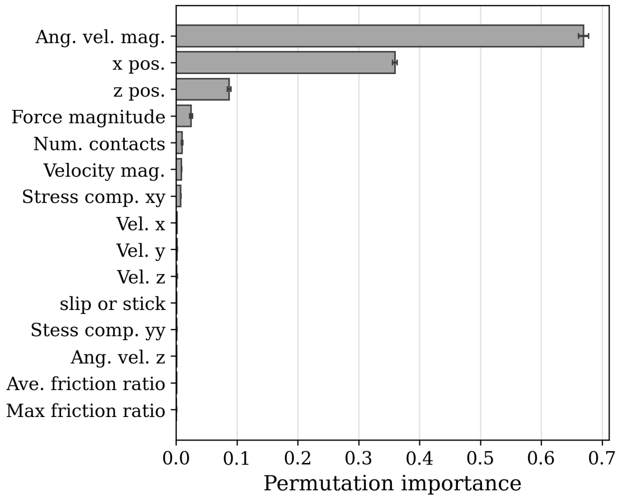

Figure 5: Feature importance of the main classification model based on permutation importance.

Table 4: Classification performance and top-ranked features for different label thresholds. The positive rate was fixed at 5% in both the training and test datasets.

Threshold	PR-AUC	Best F1	Top three features
P90	0.825	0.740	x position, angular velocity magnitude, z position
P95	0.884	0.809	angular velocity magnitude, x position, z position
P97.5	0.906	0.832	angular velocity magnitude, x position, z position
P99	0.888	0.835	angular velocity magnitude, x position, z position

features. This indicates that, even when the spatial extent of the extracted shear-band region changes, the main trend that angular velocity and spatial position strongly contribute to shear-band-particle classification is not strongly dependent on a specific label threshold. However, in the P90 case, the contribution of x position was larger than that of angular velocity. This may be because the lower threshold includes not only the main shear-band core but also surrounding deformation zones and secondary-fault-like regions, making the contribution of spatial position relatively stronger.

The results of the ablation analysis are shown in Table 5. The ablation results indicate that the classification performance does not collapse even when angular velocity, which had a high contribution in the permutation-importance analysis, is removed. This suggests that interparticle forces, contact number, friction ratio, velocity, and related features also contain information useful for classification.

Position information showed the second-highest contribution after angular velocity. This is expected because the shear band starts from the displacement-input location at the bottom and extends obliquely upward in the cross section.

Table 5: Results of the ablation analysis.

Feature set	PR-AUC	Best F1
All low-leakage features	0.908	0.835
Angular velocity removed	0.882	0.807
Position removed	0.866	0.798
Motion, force, angular velocity, and position removed	0.847	0.781
Position and angular velocity removed	0.744	0.685
Contact, stress, friction, and force features only	0.702	0.661
Contact and friction features only	0.252	0.323

In other words, the classifier uses the spatial location of the shear band to extract shear-band particles. Therefore, position information is an important feature for identifying a localized shear band. However, even when position information was removed, the PR-AUC remained 0.866, indicating that the machine-learning model could identify shear-band particles to some extent using only particle-state variables. This suggests that the classifier does not merely memorize spatial position. Furthermore, even when position and angular velocity were removed together, a certain level of classification performance remained. This quantitatively indicates that information related to force chains in granular materials, such as interparticle contact force and the number of contacts[21, 22], as well as friction-force-ratio features related to sliding states between particles, also contributes to the identification of shear-band particles.

3.5 Scope and limitations of the method

The analysis proposed in this study classifies shear-band and non-shear-band particles from particle-scale state variables at the same time step, after the shear band has already formed at that time. Therefore, this method cannot forecast shear-band initiation or infer causality. The obtained feature importances should not be interpreted as directly indicating the causes of shear-band formation; rather, they indicate particle-scale information useful for distinguishing the inside and outside of the shear band. To forecast shear-band initiation, it will be necessary to formulate a time-lagged problem in which shear-band particles at a certain time are classified using feature information from earlier times. This is a topic for future work.

4 Conclusions

This study applied a DEM model of reverse faulting and identified shear-band particles using local equivalent shear strain. Shear-band and non-shear-band particles were then classified using particle-scale features from which the shear strain itself, and displacement-derived quantities used to compute it, had been excluded.

The main conclusions are as follows. First, the classifier achieved a PR-AUC of 0.906, showing that shear-band particles sampled at unseen time steps within the same DEM condition can be identified with high classification performance even in an imbalanced particle dataset.

Second, angular velocity showed a high contribution in the feature-importance analysis. This result supports the widely discussed importance of particle rotation in shear bands.

Third, even when the shear-band-label threshold was changed to the 90th, 95th, 97.5th, and 99th percentiles and the classifier was retrained with the positive rate fixed at 5%, angular velocity magnitude, x position, and z position consistently appeared among the top-ranked features. This indicates that the main trend in feature importance obtained in this study does not depend only on the specific shear-band definition based on the 97.5th percentile.

Fourth, even when both position and angular velocity were removed, interparticle force, number of contacts, friction ratio, velocity, and related features made small but nonzero contributions to classification. These results indicate that machine-learning analysis using a low-leakage feature set for DEM particle data can serve as a quantitative tool for explaining shear-band-particle classification.

This study classified shear-band and non-shear-band particles from particle-scale features at the same time step. In other words, the method identifies particle-scale descriptors that characterize currently formed shear-band particles. Therefore, the results represent interpolation-type classification performance within a single DEM condition and do not demonstrate extrapolation to different fault angles, boundary conditions, or particle-size distributions. Future work will extend the problem to time-lagged classification, in which shear-band particles at a given time are classified using features from earlier times, in order to explore the possibility of forecasting shear-band formation.

References

[1] Ohmachi, T.: On damage to dams in Taiwan due to the 1999 Chichi earthquake, *Journal of Japan Society of Dam Engineers*, Vol. 10, No. 2, pp. 138–150, 2000.

[2] Bray, J. D., Seed, R. B., Seed, H. B. and Cluff, L. S.: Earthquake fault rupture propagation through soil, *Journal of Geotechnical Engineering*, Vol. 120, No. 3, pp. 543–561, 1994.

[3] Oda, M. and Kazama, H.: Microstructure of shear bands and its relation to the mechanisms of dilatancy and failure of dense granular soils, *Geotechnique*, Vol. 48, No. 4, pp. 465–481, 1998.

[4] Iwashita, K. and Oda, M.: Rolling resistance at contacts in simulation of shear band development by DEM, *Journal of Engineering Mechanics*, Vol. 124, No. 3, pp. 285–292, 1998.

[5] Iwashita, K. and Oda, M.: Micro-deformation mechanism of shear banding process based on modified distinct element method, *Powder Technology*, Vol. 109, pp. 192–205, 2000.

[6] Oda, M., Takemura, T. and Takahashi, M.: Microstructure in shear band observed by microfocus X-ray computed tomography, *Geotechnique*, Vol. 54, No. 8, pp. 539–542, 2004.

[7] Rechenmacher, A. L.: Grain-scale processes governing shear band initiation and evolution in sands, *Journal of the Mechanics and Physics of Solids*, Vol. 54, pp. 22–45, 2006.

[8] Cundall, P. A. and Strack, O. D. L.: A discrete numerical model for granular assemblies, *Geotechnique*, Vol. 29, No. 1, pp. 47–65, 1979.

[9] Ren, C. X., Dorostkar, O., Rouet-Leduc, B., Hulbert, C., Strebel, D., Guyer, R. A., Johnson, P. A. and Carmeliet, J.: Machine learning reveals the state of intermittent frictional dynamics in a sheared granular fault, *Geophysical Research Letters*, Vol. 46, No. 13, pp. 7395–7403, 2019.

[10] Ma, G., Mei, J., Gao, K., Zhao, J., Zhou, W. and Wang, D.: Machine learning bridges microslips and slip avalanches of sheared granular gouges, *Earth and Planetary Science Letters*, Vol. 579, 117366, 2022.

[11] Mei, J., Ma, G., Tang, L., Gao, K., Cao, W. and Zhou, W.: Spatial clustering of microscopic dynamics governs the slip avalanche of sheared granular materials, *International Journal of Plasticity*, Vol. 165, 103570, 2023.

[12] Wang, M., Kumar, K., Feng, Y. T., Qu, T. and Wang, M.: Machine learning aided modeling of granular materials: A review, *Archives of Computational Methods in Engineering*, Vol. 32, pp. 1997–2034, 2025.

[13] Fransen, M. et al.: Towards scientific machine learning for granular material simulations: Challenges and opportunities, *Archives of Computational Methods in Engineering*, Vol. 33, pp. 789–821, 2026.

[14] Kloss, C., Goniva, C., Hager, A., Amberger, S. and Pirker, S.: Models, algorithms and validation for open-source DEM and CFD–DEM, *Progress in Computational Fluid Dynamics*, Vol. 12, No. 2–3, pp. 140–152, 2012.

[15] Bagi, K.: Stress and strain in granular assemblies, *Mechanics of Materials*, Vol. 22, No. 3, pp. 165–177, 1996.

[16] Friedman, J. H.: Greedy function approximation: A gradient boosting machine, *The Annals of Statistics*, Vol. 29, No. 5, pp. 1189–1232, 2001.

[17] Pedregosa, F. et al.: Scikit-learn: Machine learning in Python, *Journal of Machine Learning Research*, Vol. 12, pp. 2825–2830, 2011.

[18] Saito, T. and Rehmsmeier, M.: The precision-recall plot is more informative than the ROC plot when evaluating binary classifiers on imbalanced datasets, *PLOS ONE*, Vol. 10, No. 3, e0118432, 2015.

[19] Breiman, L.: Random forests, *Machine Learning*, Vol. 45, pp. 5–32, 2001.

[20] Fisher, A., Rudin, C. and Dominici, F.: All models are wrong, but many are useful: Learning a variable's importance by studying an entire class of prediction models simultaneously, *Journal of Machine Learning Research*, Vol. 20, No. 177, pp. 1–81, 2019.

[21] Radjai, F., Wolf, D. E., Jean, M. and Moreau, J. J.: Bimodal character of stress transmission in granular packings, *Physical Review Letters*, Vol. 80, No. 1, pp. 61–64, 1998.

[22] Peters, J. F., Muthuswamy, M., Wibowo, J. and Tordesillas, A.: Characterization of force chains in granular material, *Physical Review E*, Vol. 72, 041307, 2005.